# Controlling Surface Reactions with Nanopatterned Surface Elastic Strain

**Zhisheng Li, Denis V. Potapenko, and Richard M. Osgood***

Laboratory for Light Surface Interactions, Department of Applied Physics and Applied Mathematics, Columbia University, New York, New York 10025, United States

**ABSTRACT** The application of elastic lattice strain is a promising approach for tuning material properties, but the attainment of a systematic approach for introducing a high level of strain in materials so as to study its effects has been a major challenge. Here we create an array of intense locally varying strain fields on a $TiO_2$ (110) surface by introducing highly pressurized argon nanoclusters at 6−20 monolayers under the surface. By combining scanning tunneling microscopy imaging and the continuum mechanics model, we show that strain causes the surface bridge-bonded oxygen vacancies (BBOv), which are typically present on this surface, to be absent from the strained area and generates defect-free regions. In addition, we find that the adsorption energy of hydrogen binding to oxygen (BBO) is significantly altered by local lattice strain. In particular, the adsorption energy of hydrogen on BBO rows is reduced by ∼35 meV when the local crystal lattice is compressed by ∼1.3%. Our results provide direct evidence of the influence of strain on atomic-scale surface chemical properties, and such effects may help guide future research in catalysis materials design.

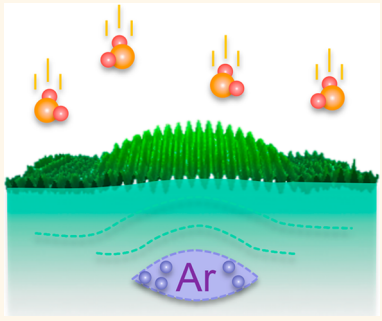


**KEYWORDS:** $TiO_2$ · STM · strain · BBOv · adsorption

Elastic strain is commonly present in nanostructured surfaces[1,2] and on supported catalysts.[3] In addition, strain has been found to change chemical and electronic properties in a broad range of material systems. For example, charge carrier mobility is significantly increased due to lattice strain in epitaxial silicon.[4,5] On metal surfaces, the energetics of adsorption and dissociation of molecular adsorbates can also be greatly altered through surface strain.[6−9] Despite its prevalence, the role of strain in altering chemisorption is a major unanswered question in heteroreaction systems. An important issue in catalytic studies of strain is the degree to which strain in a substrate will affect chemisorption of molecular species on that surface. This paper reports the role of strain in surface reactivity for single-crystal $TiO_2$, an important two-component semiconducting oxide crystal, which is of intense interest due to its promising applications including photocatalysis,[10] gas sensors,[11] solar cells,[12,13] and others.[14] Strain is known to play a key role in several of these applications: for example, in hydrogenated black $TiO_2$,[15,16] strain appears during its high-pressure processing and the resulting disordered outer layer is believed to be responsible for midgap states in the crystal, which enhances optical adsorption of visible and infrared light. The role of strain in many of these cases remains an open question. One limitation to addressing this question is the experimental difficulty in generating significant strain fields and distinguishing the effect of this strain from chemistry due to other changes in surface properties.

Our approach to generate controllable strain fields is based on recent experiments in our laboratory, which have shown that bombarding a single-crystal $TiO_2$ (110) sample with low-energy (1 kV) argon ions at an elavated temperature will produce an array of nanoscale areas of subsurface argon clusters.[17] In particular, our studies have found that resulting intersitial argon atoms migrate and accumulate in a subsurface region 6−20 monolayers below the surface, forming highly pressurized nanoclusters. As a consequence, the thin surface layer above these clusters protrudes or bulges outward to form a blister-like nanofeature, thus generating a large-value local strain field, which is ideal for the surface reactivity experiments examined here. Note that although studies about noble gas bubbles in metal oxides are relatively scarce, nanobubbles of high pressure noble gases are well known in metal systems based on studies of plasma wall interactions.[18]

* Address correspondence to osgood@columbia.edu.

Received for review October 28, 2014 and accepted December 10, 2014.

**Published online December 10, 2014**
10.1021/nn506150m

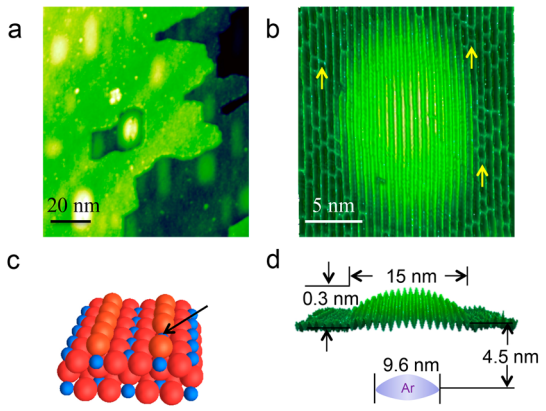


**Figure 1. Surface protrusions after argon bombardment. (a) $TiO_2$ (110) surface after argon-ion bombardment. (b) One typical example of a protrusion. Bridge-bonded oxygen vacancies (BBOvs) are marked by yellow arrows on flat areas. These vacancies are not present at the top of the protrusion. (c) Ball model of rutile (110) surface with a BBO vacancy, marked by a black arrow. (d) Side view of image b, along with a sketch of the depth and diameter of the corresponding subsurface argon clusters, simulated by the continuum mechanics model.**

In addition, subsurface argon nanoclusters introduced by bombardment of low-energy argon ions have also been observed in metal systems, including Al, Cu, and Ru,[7,19,20] where argon nanoclusters were found with similar size and depth to those observed in our experiments.

## RESULTS AND DISCUSSION

**Locally Varying Strain Field.** Prior to examining issues of surface reactivity, the surface of a single-crystal rutile $TiO_2$ sample was prepared through bombardment with 1 kV argon ions at 900 K for 10 min. Figure 1a shows an image of such a $TiO_2$ (110) surface after argon-ion bombardment. Due to the subsurface argon clusters, locally deformed $TiO_2$ regions, *i.e.*, surface protrustions, appear as bright ellipses in our scanning tunneling microscopy (STM) image. As the image in Figure 1a shows, most of the protrusions are enlongated along the [001] direction due to the anisotropy in the stress tensor along different crystal orientations.[21] One important feature to note is that most of the protrusions retain their flat-surface-layer crystal structure despite the excessive stress that is obviously present; one clear example is shown in Figure 1b. However, in Figure 1a there are surfaces of protrusions that have undergone a more significant local surface reconstruction (or more precisely the removal of 2 or 3 atomic rows). We attribute this reconstructed surface structure to the excess stress present on protrusions, which exceeds the elastic limit.

Measurements within the STM images showed that the lateral dimensions of the protrusions range from 8 to 20 nm and the height can reach up to 1 nm. Note that the height of the protrusions was found not to vary with a change in scanning bias voltage. Therefore, the possbiliby that these protrusions are due to local electronic effects can be excluded. Figure 1b shows a higher-resolution image of the surface, which includes one example of a protrusion. A side view of the STM image, along with a schematic drawing of the corresponding subsurface argon cluster, which is determined from a continuum mechanics model (see more details in ref 17), is shown in Figure 1d.

In the examination of our images, such as Figure 1b, we observed that there were subtle but important nonuniformities in the distribution of oxygen vacancies (bridge-bonded oxygen vacancies, BBOv; schematically shown in Figure 1c) across the crystal surface. As shown in Figure 1b, oxygen vacancies appear as bright protrusions on the dark BBO atomic rows on a flat surface area; for clarity, several of these BBOvs are marked with yellow arrows. Also note that oxygen vacancies and OH groups were clearly distinguishable from each other in our STM images, such that OH groups appear round and bright, while oxygen vacancies are bridge-like and paler. Thus, the bridge-like features in Figure 1b can be confidently attributed to oxygen vacancies. The surface preparation of the sample used for this figure resulted in the formation of ~12% oxygen vacancies on typical planar areas of the surface. In contrast, oxygen vacancies are completely absent on the surface of the protruding area. In fact, we have performed close examinations on more than 20 protrusions, in which BBOvs were clearly identified and all protrusions were found to be free of BBOvs

Typically these BBO vacancies are formed on a virgin $TiO_2$ (110) surface by annealing to high temperature in a vacuum. The density of these oxygen vacancies depends on both the annealing temperature and annealing time. For transition-metal oxides, such oxygen vacancies are known to be important point defects, which are intrinsically coupled with magnetic,[22] electronic,[23] and transport properties of materials. In the case of $TiO_2$, these sites have been reported to cause water dissociation,[10] alcohol dehydration, *etc.*[14] Obtaining experimental access to vary the concentration of oxygen vacancies as well as their spatial distribution can provide a major "tool" for the design of catalytic materials. To our knowledge, very limited theoretical and experimental studies have been reported on how strain affects oxygen-vacancy formation and migration. Among the existing studies, it has been shown that by applying in-plane tensile/compressive strain, it is possible to alter the energetics for creating oxygen vacancies and to lower substantially the oxygen-vacancy migration barrier.[24,25] Although our results do not conclusively show whether the absence of oxygen vacancies on the strained area is a thermal-equilibrium state or a kinetic-limited resulting state, we do show clearly that the oxygen-vacancy distribution can be tuned by stress/strain. This approach may provide a path to controlled decoration of a $TiO_2$ surface through oxygen-vacancy patterning.

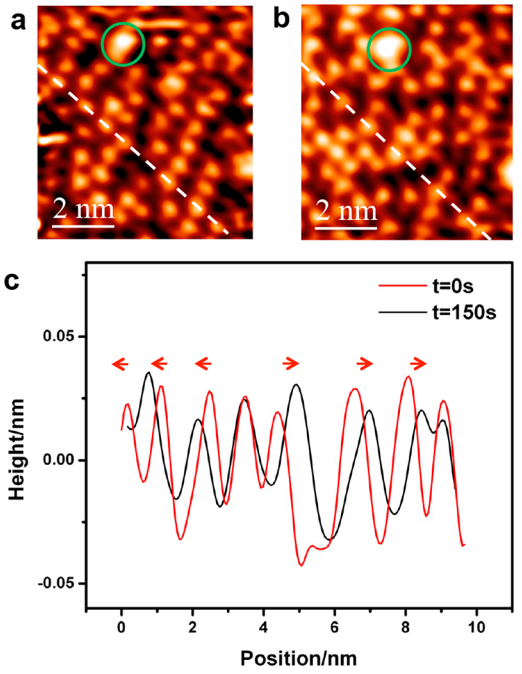


**Figure 2. Diffusion of surface OH groups. STM images of the same area: (a) $t = 0$ s; (b) $t = 150$ s to illustrate the distribution and diffusion of hydrogen. (c) Line profiles of the same BBO rows. The bright feature marked with a circle is a solid impurity, which was immobile and was used as a reference point. During the time of examination, most hydrogen atoms diffused away from their original absorption sites, indicating high mobility at room temperature.**

**Experiments Using Water-Vapor Dosing.** To further study the effect of strain on surface adsorption, we conducted a water-vapor-exposure experiment. $H_2O$ absorption on our BBOv patterned surface provides a particularly clear example of how strain may influence chemisorption on the $TiO_2$ surface. In our experiments, ~10 L of $H_2O$ vapor was dosed on the surface at room temperature. Many earlier studies have shown that $H_2O$ molecules adsorb dissociatively on BBOv sites, with the oxygen atom filling the BBOv and with one H−O bond broken such that a hydrogen atom attaches to an adjacent BBO.[26,27] This process forms a pair of two adjacent bridging OH groups, which are free to migrate on the surface.[28] After exposing our $TiO_2$ surface to water vapor, our STM images show that the BBOvs are then fully refilled by water molecules. Thus, after exposure, the final surface is covered by hydrogen atoms bonded to a BBO rows of $TiO_2$ (110). Filling of BBOvs also has the other important result of limiting any uneven distribution of charges associated with BBOvs, which in turn can influence the diffusion of OH groups.

Figure 2a shows an STM image obtained from a planar area of the surface after water exposure. In the image, the OH groups derived from the $H_2O$ dissociation appear as bright dots on the BBO rows. The resulting surface OH groups are evenly distributed across the surface. This even distribution is attributed to H−H repulsion such as seen in surface diffusion

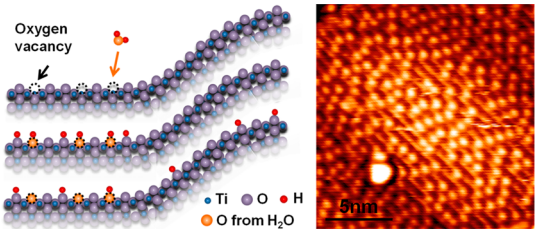


**Figure 3. A protrusion covered with surface OH groups after water exposure. Left: Schematics of $H_2O$ dissociative adsorption at BBOv on planar areas and diffusion to the top of the protrusion afterward. Right: Atomic-resolution STM image of a protrusion after water exposure. Hydrogen covers both the flat areas and the surface of the protrusion.**

measurements.[28] Thus, this uniform distribution is a consequence of the fact that these hydrogen atoms exhibit simple Coulomb repulsion rather than the complex structure-related interparticle interactions that dominate other cases of adsorption process.[29,30]

We can examine the mobility of OH groups derived from $H_2O$ dissociation by comparing consecutive STM images as seen in Figure 2. During the time that these two images were taken, most hydrogen atoms diffused away from their original positions. Their high mobility ensures that the observed OH distributions reached a thermal equilibrium state, which is critical for thermal-statistic analysis performed later on.

Figure 3 shows an image of a protrusion after the surface has been dosed with water vapor. Notice that after exposure, the top of the protrusion was covered with OH groups, despite the fact that the protrusion was free of BBOvs before water exposure. This observation further confirms that hydrogen atoms are mobile at room temperature, since our observations suggest that they migrate to the top of the protrusions after being produced on the flat terraces. Quantitative examination (see below) of the STM images reveals that H concentration on the protrusion is lower than that on flat terraces. Furthermore, H concentration on the protrusion has a nonuniform distribution.

In order to quantitatively analyze the data, plots of the OH concentration across the protrusion along the [1−10] direction were made, as shown in Figure 4. In this plot, a window of surface sample width of 6 nm was selected for study to minimize the local concentration fluctuation. Six consecutive images of the same area were averaged to get the final OH concentration distribution. The time interval between images was ~5 min. As just discussed, the positions of OH groups change from image to image, and the final distribution is thus an equilibrium distribution, which directly reflects local variations in adsorption energy,[9] as well as temporal fluctuations due to the stochastic nature of the diffusion process.

In addition to a plot of the local OH concentration, Figure 4 also shows the calculated radial strain along the [1−10] direction and across the center of the protrusion, calculated from the continuum mechanics

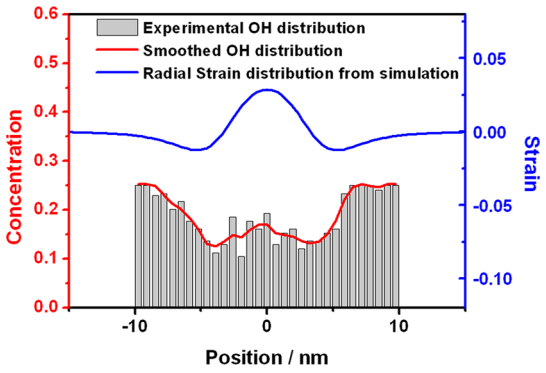


**Figure 4. Plot of hydrogen distribution at the top of protrusion along with the local radial strain on the surface of the protrusion calculated from the continuum mechanics model. A positive strain indicates an area with lattice expansion, and a negative strain indicates an area with lattice compression. Hydrogen distribution follows the overall "W"-shape trend that the strain exhibits.**

model. The positive value of strain shows that the crystal lattice expands at the center of the protrusion. In the most highly strained area, the local lattice expansion reaches ~3%. At the edge of the protrusion, the crystal lattice is compressed (negative strain) to nearly 1.3%; this compression is a result of concave bending of surface layers. Both the radial strain and the OH concentration exhibit a "W"-shaped behavior for each of these quantities *versus* radial coordinate. This similarity in behavior shows the close correlation between strain and OH binding energy.

On going from a flat terrace to the edge of a protrusion, the surface lattice is gradually compressed and the OH concentration decreases and reaches a minimum (~13% *vs* ~25% on flat terraces) where the surface lattice is maximally compressed. For mobile adsorbates on a nonuniformly strained area, the expected occupation probability of different sites is given by $p = p_0 e^{-(\Delta E_a/kT)}$, where $p_0$ denotes the occupation probability of a reference site and $\Delta E_a$ the adsorption energy difference compared to the reference site.[9] Since the high mobility of hydrogen atoms assures that different adsorbing areas are in thermal equilibrium with each other, the occupation probability is directly related to the local concentration or coverage; thus $\theta = \theta_0 e^{-(\Delta E_a/kT)}$, where $\theta_0$ is hydrogen coverage at flat terraces, which is chosen here to be the reference site. To obtain a quantitative estimation of the strain effects on adsorption energy, the most compressed region was chosen to provide a comparison with a flat terrace region. Substituting the different hydrogen coverage gives $\Delta E_a = 17$ meV for the overall adsorption energy difference at these two regions.

The overall adsorption energy difference ($\Delta E_a$) originates from two sources: the change in the H−H repulsion energy ($\Delta E_r$) due to different coverage, and the change in the surface binding energy resulting from local strain ($\Delta E_s$), which can be summarized as the following: $\Delta E_s = \Delta E_a - \Delta E_r$. To obtain the strain-related energy difference ($\Delta E_s$), the measurement of $\Delta E_r$ is discussed below.

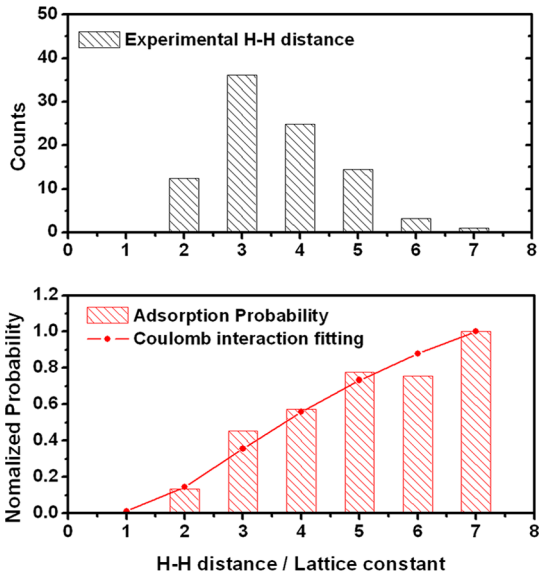


**Figure 5. H−H repulsion analysis. Upper panel: H−H separation distribution as a function of $TiO_2$ (110) surface lattice constant. Lower panel: Normalized H−H adsorption probability and corresponding Coulomb interaction fitting.**

**Analysis of H−H Repulsion.** Since H−H interaction also affects the final distribution of H, we also performed analysis on H−H repulsion; this analysis allowed us to extract the effects solely due to substrate strain. After exposure to water, the surface coverage of H is ~25%, as each water molecule produces two OH groups upon adsorption at BBOv sites (~12%). In this process, partial charge is transferred from a H atom to a BBO row. The positively charged H then experiences repulsion from its H neighbors, which decreases monotonically as the H−H separation distance increases, an effect explored in other studies.[28] The upper panel of Figure 5 shows the H−H separation as a function of surface lattice constant, which is acquired through statistical analysis of STM images on planar areas of $TiO_2$ (110). It is worth noting that the probability shown here is not an absolute adsorption probability, $p_n$, but rather a conditional adsorbing probability, $P_n = p_n \prod_{m=1}^{n-1}(1 - p_m)$, which is to say it is the probability of hydrogen adsorbing at the $n$th neighbor when no hydrogen is found at previous neighbors; thus,

$$P_1 = p_1$$

$$P_2 = p_2 \times (1 - p_1)$$

$$P_3 = p_3 \times (1 - p_1) \times (1 - p_2) = p_3 \times (1 - P_1 - P_2)$$

$$\vdots$$

$$P_n = p_n \times (1 - p_1) \times \cdots \times (1 - p_{n-1})$$

$$= p_n \times (1 - \sum_{m=1}^{n-1} P_m)$$

To get the absolute adsorbing probability $p_n$, eq 1 is used.

$$p_n = P_n/(1 - \sum_{m=0}^{n-1} P_m) \quad (1)$$

The resulting absolute adsorption probabilities are shown in the lower panel of Figure 5, which are normalized by the highest value. The adsorption probability distribution can easily be understood as that due to the repulsion between OH groups; the further two OH's are separated, the higher the adsorption probability. We fitted the adsorption probability with a simple charge−charge Coulomb interaction. The H−H displacement probability is directly related to the repulsion energy through eq 2:

$$p_n \propto e^{-E_{r_n}/kT} \quad (2)$$

where $E_{r_n} = (Q^2/4\pi\varepsilon r_n^2)$ is the repulsion energy when two hydrogen are separated by $n$ lattice constants, $Q$ is the fractional charge residing on hydrogen, $k$ is Boltzmann's constant, $r_n$ is the distance between hydrogens at the $n$th neighbor, and $T$ is temperature, which is room temperature in our case. The fractional charge, $Q$, is the only parameter used in the fitting. The inter-row interaction is considered negligible for influencing the H−H in-row displacement distribution, since the repulsions experienced from two sides of the row are canceled.

The fractional charge on the H atom, which was determined from the fitting, is 0.17$e$. Therefore, for ∼13% (25%) of hydrogen coverage, the average H−H separation distance is ∼8 (4) lattice constant, and the repulsion energy difference for these two configurations is found to be $\Delta E_r = -18$ meV. The surface binding energy difference, which can be attributed exclusively to strain, can then be estimated as $\Delta E_s = \Delta E_a - \Delta E_r = 35$ meV. Note that in calculating H−H repulsion the same local charge for H atoms was assumed for flat and for strained areas, because this strain-induced deviation of the local charge can be only a small fraction of the total local charge on H atoms, just as the strain-induced deviation of the O−H bond strength ($\Delta E = 35$ meV) is a small fraction of the bond strength itself (∼3.86 eV).[31] Therefore, the charge difference of H atoms at flat areas and strained areas (∼35 meV/3.86 eV < 1%) can be safely neglected in our study.

Thus, when the crystal lattice is compressed by 1.3%, the binding energy of OH is reduced by 35 meV. This energy difference between strained and unstrained surfaces is comparable to the thermal energy at room temperature (∼25 meV), and thus it is expected to affect adsorption, diffusion, and distribution significantly.

Note that on going from the compressed region to the most expanded region (the top of the protrusion), the OH concentration is again found to increase. As the top and the edge of the protrusion show different polarity of strain, a "reversed" chemical effect is expected at the top of the protrusion; thus the OH concentration is expected to be higher on the top than that on the flat terraces. However, this behavior is not observed in the experiment. One possible explanation is that the layers of $TiO_2$ above the argon clusters are isolated from the rest of the bulk by the presence of argon atoms. The confinement of electrons in this layer may impose a secondary effect on H distribution across the protrusion. More theoretical and experimental studies are required to understand this effect in detail.

## CONCLUSIONS

To summarize, we have introduced a method to form a locally varying strain field on rutile $TiO_2$ (110) surfaces through pressurized subsurface argon nanoclusters. With this surface, we have demonstrated a strongly strain-altered surface chemistry. In particular, STM imaging shows that oxygen vacancies, which are typically present on this surface, are fully absent from the strained regions of the surface. Also, we observed that the binding energy of adsorbates is controlled by the local strain. Specifically, using statistical analysis of STM images, we show that the adsorption energy of hydrogen on BBO rows is reduced by ∼35 meV when the local crystal lattice is compressed by ∼1.3%. Our experimental findings provide insight into the role of strain in driving surface reactions.

## METHODS

All experiments were conducted in a customized UHV chamber, with a base pressure of $4 \times 10^{-11}$ Torr, which was equipped with an Omicron VT-STM, a combined LEED/Auger system, and an Ar-ion sputtering gun. A single-crystal 5 × 5 × 1 mm, rutile $TiO_2$ (110) sample was mounted on a commercial Omicron sample holder. The sample was attached to the Mo surface of a custom-built heating plate with Ta wires; silver powder was used as a contact layer to enhance heat conduction from the heating plate to the sample. A K-type thermocouple was attached to the edge of the sample to monitor the sample temperature. To generate stressed surface protrusions, the sample was bombarded with 1 keV argon ions at an elevated temperature (900 K) for 10 min. The ion gun produced argon-ion currents of ∼5 $\mu$A at the sample surface. Experiments with precise water exposure were administered through an aperture-based gas system, in which the gas line, before a 5 $\mu$m aperture, was filled with water vapor in the mTorr pressure range for a desired amount of time. The other side of the aperture was opened to a 4 mm diameter tube leading toward the sample; the latter faced the UHV-side opening of this tube with a ∼5 mm distance. We used a continuum mechanics model to simulate the surface deformation and strain distribution. More details can be found in our previous publication.[17]

*Conflict of Interest:* The authors declare no competing financial interest.

*Acknowledgment.* This work is supported by the Basic Energy Sciences Division of the U.S. Department of Energy, Contract No. DE-FG02-90ER14104. We thank Professor Jeffery W.

Kysar and Nader Zaki for very helpful discussions. In addition the stages of this work, particularly on surface decoration by H, were supported by NSF-DMR Contract No. DMR-1206768.

## REFERENCES AND NOTES


1. Gilbert, B.; Huang, F.; Zhang, H. Z.; Waychunas, G. A.; Banfield, J. F. Nanoparticles: Strained and Stiff. *Science* **2004**, *305*, 651–654.
2. Strasser, P.; Koh, S.; Anniyev, T.; Greeley, J.; More, K.; Yu, C. F.; Liu, Z. C.; Kaya, S.; Nordlund, D.; Ogasawara, H.; *et al*. Lattice-Strain Control of the Activity in Dealloyed Core-Shell Fuel Cell Catalysts. *Nat. Chem.* **2010**, *2*, 454–460.
3. Schlapka, A.; Lischka, M.; Groß, A.; Käsberger, U.; Jakob, P. Surface Strain Versus Substrate Interaction in Heteroepitaxial Metal Layers: Pt on Ru(0001). *Phys. Rev. Lett.* **2003**, *91*, 016101.
4. Thompson, S. E.; Armstrong, M.; Auth, C.; Alavi, M.; Buehler, M.; Chau, R.; Cea, S.; Ghani, T.; Glass, G.; Hoffman, T.; *et al*. A 90-nm Logic Technology Featuring Strained-Silicon. *IEEE Trans. Electron Devices* **2004**, *51*, 1790–1797.
5. Sun, Y.; Thompson, S. E.; Nishida, T. *Strain Effect in Semiconductors: Theory and Device Applications*; Springer: New York, 2010; p 1−350.
6. Goikoetxea, I.; Juaristi, J.; Muiño, R. D.; Alducin, M. Surface Strain Improves Molecular Adsorption but Hampers Dissociation for $N_2$ on the Fe/W (110) Surface. *Phys. Rev. Lett.* **2014**, *113*, 066103.
7. Gsell, M.; Jakob, P.; Menzel, D. Effect of Substrate Strain on Adsorption. *Science* **1998**, *280*, 717–720.
8. Mavrikakis, M.; Hammer, B.; Nørskov, J. K. Effect of Strain on the Reactivity of Metal Surfaces. *Phys. Rev. Lett.* **1998**, *81*, 2819–2822.
9. Jakob, P.; Gsell, M.; Menzel, D. Interactions of Adsorbates with Locally Strained Substrate Lattices. *J. Chem. Phys.* **2001**, *114*, 10075–10085.
10. Fujishima, A.; Honda, K. Electrochemical Photolysis of Water at a Semiconductor Electrode. *Nature* **1972**, *238*, 37–38.
11. Mor, G. K.; Carvalho, M. A.; Varghese, O. K.; Pishko, M. V.; Grimes, C. A. A Room-Temperature $TiO_2$-Nanotube Hydrogen Sensor Able to Self-Clean Photoactively from Environmental Contamination. *J. Mater. Res.* **2004**, *19*, 628–634.
12. Bach, U.; Lupo, D.; Comte, P.; Moser, J.; Weissörtel, F.; Salbeck, J.; Spreitzer, H.; Grätzel, M. Solid-State Dye-Sensitized Mesoporous $TiO_2$ Solar Cells with High Photon-to-Electron Conversion Efficiencies. *Nature* **1998**, *395*, 583–585.
13. Gratzel, M. Photoelectrochemical Cells. *Nature* **2001**, *414*, 338–344.
14. Diebold, U. The Surface Science of Titanium Dioxide. *Surf. Sci. Rep.* **2003**, *48*, 53–229.
15. Chen, X. B.; Liu, L.; Yu, P. Y.; Mao, S. S. Increasing Solar Absorption for Photocatalysis with Black Hydrogenated Titanium Dioxide Nanocrystals. *Science* **2011**, *331*, 746–750.
16. Liu, L.; Peter, Y. Y.; Chen, X.; Mao, S. S.; Shen, D. Hydrogenation and Disorder in Engineered Black $TiO_2$. *Phys. Rev. Lett.* **2013**, *111*, 065505.
17. Potapenko, D. V.; Li, Z.; Kysar, J. W.; Osgood, R. M. Nanoscale Strain Engineering on the Surface of a Bulk $TiO_2$ Crystal. *Nano Lett.* **2014**, *14*, 6185–6189.
18. Trinkaus, H. Energetics and Formation Kinetics of Helium Bubbles in Metals. *Radiat. Eff.* **1983**, *78*, 189–211.
19. Schmid, M.; Hebenstreit, W.; Varga, P.; Crampin, S. Quantum Wells and Electron Interference Phenomena in Al Due to Subsurface Noble Gas Bubbles. *Phys. Rev. Lett.* **1996**, *76*, 2298.
20. Kurnosikov, O.; Adam, O.; Swagten, H.; de Jonge, W.; Koopmans, B. Probing Quantum Wells Induced above a Subsurface Nanocavity in Copper. *Phys. Rev. B* **2008**, *77*, 125429.
21. Wachtman, J. B.; Tefft, W. E.; Lam, D. G. Elastic Constants of Rutile ($TiO_2$). *J. Res. Natl. Stand. Sect. A* **1962**, *66*, 465–471.
22. Scott, J.; Dawber, M. Oxygen-Vacancy Ordering as a Fatigue Mechanism in Perovskite Ferroelectrics. *Appl. Phys. Lett.* **2000**, *76*, 3801–3803.
23. Yang, J. J.; Pickett, M. D.; Li, X.; Ohlberg, D. A.; Stewart, D. R.; Williams, R. S. Memristive Switching Mechanism for Metal/Oxide/Metal Nanodevices. *Nat. Nanotechnol.* **2008**, *3*, 429–433.
24. Shu, D.-J.; Ge, S.-T.; Wang, M.; Ming, N.-B. Interplay between External Strain and Oxygen Vacancies on a Rutile $TiO_2$(110) Surface. *Phys. Rev. Lett.* **2008**, *101*, 116102.
25. Wang, Z. W.; Shu, D. J.; Wang, M.; Ming, N. B. Strain Effect on Diffusion Properties of Oxygen Vacancies in Bulk and Subsurface of Rutile $TiO_2$. *Surf. Sci.* **2012**, *606*, 186–191.
26. Bikondoa, O.; Pang, C. L.; Ithnin, R.; Muryn, C. A.; Onishi, H.; Thornton, G. Direct Visualization of Defect-Mediated Dissociation of Water on $TiO_2$(110). *Nat. Mater.* **2006**, *5*, 189–192.
27. Schaub, R.; Thostrup, P.; Lopez, N.; Lægsgaard, E.; Stensgaard, I.; Nørskov, J. K.; Besenbacher, F. Oxygen Vacancies as Active Sites for Water Dissociation on Rutile $TiO_2$(110). *Phys. Rev. Lett.* **2001**, *87*, 266104.
28. Li, S. C.; Zhang, Z.; Sheppard, D.; Kay, B. D.; White, J. M.; Du, Y.; Lyubinetsky, I.; Henkelman, G.; Dohnalek, Z. Intrinsic Diffusion of Hydrogen on Rutile $TiO_2$(110). *J. Am. Chem. Soc.* **2008**, *130*, 9080–9088.
29. Potapenko, D. V.; Choi, N. J.; Osgood, R. M. Adsorption Geometry of Anthracene and 4-Bromobiphenyl on $TiO_2$-(110) Surfaces. *J. Phys. Chem. C* **2010**, *114*, 19419–19424.
30. Whitesides, G.; Mathias, J.; Seto, C. Molecular Self-Assembly and Nanochemistry: A Chemical Strategy for the Synthesis of Nanostructures. *Science* **1991**, *254*, 1312–1319.
31. Leconte, J.; Markovits, A.; Skalli, M. K.; Minot, C.; Belmajdoub, A. Periodic ab Initio Study of the Hydrogenated Rutile $TiO_2$(110) Surface. *Surf. Sci.* **2002**, *497*, 194–204.